Dalton Transactions

An international journal of inorganic chemistry

www.rsc.org/dalton

Number 40 | 28 October 2008 | Pages 5389–5512

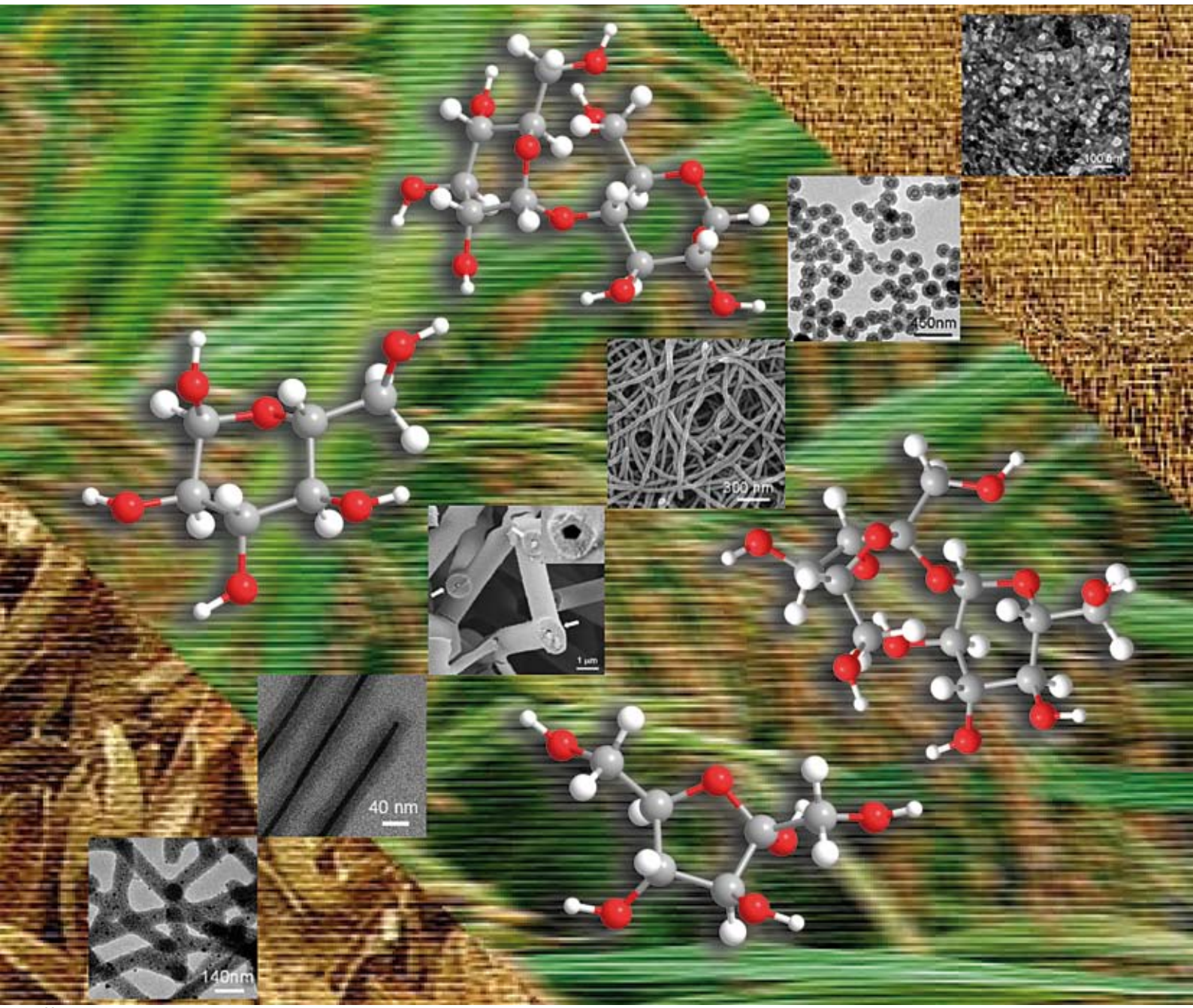

ISSN 1477-9226

RSC Publishing

1477-9226(2008)40;1-1

This paper is published as part of a *Dalton Transactions* theme issue on:

Nanomaterials for alternative energy sources

Guest editor: Andrew Barron
Rice University, Houston, Texas, USA

Published in issue 40, 2008 of *Dalton Transactions*

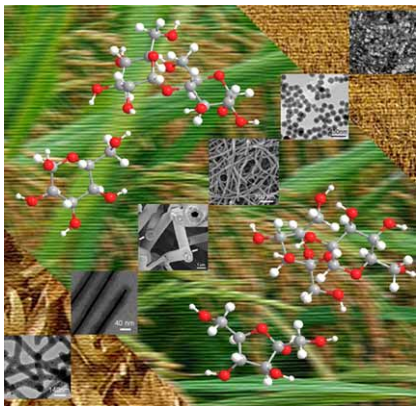

Image reproduced by permission of Shu-Hong Yu

Other papers published in this issue include:

Nanostructured thin solid oxide fuel cells with high power density
Alex Ignatiev, Xin Chen, Naijuan Wu, Zigui Lu and Laverne Smith, *Dalton Trans.,* 2008, DOI: 10.1039/b805658g

Inorganic nanomaterials for batteries
M. Stanley Whittingham, *Dalton Trans.,* 2008, DOI: 10.1039/b806372a

Raman spectroscopy of charge transfer interactions between single wall carbon nanotubes and [FeFe] hydrogenase
Jeffrey L. Blackburn, Drazenka Svedruzic, Timothy J. McDonald, Yong-Hyun Kim, Paul W. King and Michael J. Heben, *Dalton Trans.,* 2008, DOI: 10.1039/b806379f

Shape control of inorganic materials *via* electrodeposition
Kyoung-Shin Choi, *Dalton Trans.*, 2008, DOI: 10.1039/b807848c

Visit the *Dalton Transactions* website for more cutting-edge inorganic materials research
www.rsc.org/dalton

Functional carbonaceous materials from hydrothermal carbonization of biomass: an effective chemical process

Bo Hu, Shu-Hong Yu,* Kan Wang, Lei Liu and Xue-Wei Xu

Received 18th March 2008, Accepted 18th April 2008
First published as an Advance Article on the web 26th June 2008
DOI: 10.1039/b804644c

Recently, much attention has been attracted to the use of biomass to produce functional carbonaceous materials from the viewpoint of economic, environmental and societal issues. Among different techniques, the hydrothermal carbonization (HTC) process, a traditional but recently revived method, presents superior characteristics that make it a promising route of wide potential application. This perspective gives an overview of the latest advances in the HTC process of functional carbonaceous materials from biomass. First, we discuss the preparation of carbonaceous materials synthesized by the use of either highly directed or catalyst/template-assisted methods, from crude plant materials and carbohydrates respectively. These carbonaceous materials not only have special morphologies, such as nanospheres, nanocables, nanofibers, submicrocables, submicrotubes and porous structures, but also contain rich functional groups which can greatly improve hydrophilicity and chemical reactivity. Further, a general look is cast on the applications of this kind of carbonaceous materials in environmental, catalytic and electrical areas. Recent advances have demonstrated that the HTC process from biomass can provide promising methods for the rational design of a rich family of carbonaceous and hybrid functional carbon materials with important applications.

1. Introduction

Since the discovery of fullerenes[1] and carbon nanotubes,[2] the synthesis of functional carbonaceous materials has been a hot topic, motivated by its potential importance in catalyst supports, carbon fixation, adsorbents, gas storage, electrode, carbon fuel cells and drug delivery.[3] Foremost among the research changes is the shifting of the production of carbonaceous materials and energy from fossil fuels to biomass. Biomass, because of its low value, huge amount, rapid regeneration, easy access and environmental friendship, has a qualification as a promising starting material for the synthesis of these functional carbonaceous materials in spite of the debates among many scientists and engineers upon biofuels,[4] bioenergy[5] and biomaterials.[6]

Yet, whether the biomass conversion system is thermochemical or biological, there still doesn't appear to be a satisfactory and optimal process.[7] Besides, the traditional synthesis of carbon materials *via* hydrothermal carbonization always relies on harsh conditions,[8] *e.g.* carbon nanofibers have been prepared under a high temperature (up to 800 °C) and high pressure (up to 100 MPa).[9] In contrast, solvothermal carbonization prevailing recent years usually relies on organic and volatile solvents.[10,11] As an alternative, the hydrothermal carbonization (HTC) process reviving recently, however, has great potential to function as

Division of Nanomaterials & Chemistry, Hefei National Laboratory for Physical Sciences at Microscale, University of Science and Technology of China, Hefei, P. R. China. E-mail: shyu@ustc.edu.cn; Fax: +86 (0)551 3603040

Bo Hu

Bo Hu received his BS degree in 2002 and MS degree in 2005, both in chemical engineering and technology from Hefei University of Technology, and finally his PhD in chemistry from the University of Science and Technology of China in 2008 supervised by Prof. Shu-Hong Yu. He is interested in the synthesis of carbonaceous materials by hydrothermal carbonization processes from biomass, the carbonization mechanism and the self-assembly of nanoparticles.

Shu-Hong Yu

Shu-Hong Yu received his PhD in 1998, joined the Tokyo Institute of Technology in 1999 and then the Max Planck Institute (2001–2). Appointed Cheung Kong Professor in 2006, he now leads the Division of Nanomaterials & Chemistry at USTC. Research interests include bioinspired synthesis and the self-assembly of nanostructured materials. He is a board member of Current Nanoscience *and* Chinese Journal of Inorganic Chemistry.

the most promising route for its intrinsic properties, such as high carbon efficiency[3b] under mild conditions (≤200 °C), and abundant functional groups remaining on the product surface.[3b,12]

In retrospect the HTC process, an environmentally friendly route that uses water as solvent and proceeds in a sealed reaction container under a controlled temperature between 100 and 200 °C, has evolved over a long history.[13] In 1913, Bergius[13a] first described the hydrothermal transformation of cellulose into coal-like materials and early works mainly focus on the preparation of biofuels from biomass.[13] More recently, the HTC process has been used for the synthesis of uniform carbon spheres using sugar or glucose as precursors under mild conditions (≤ 200 °C) at the beginning of the new century.[14,15] Subsequently, a variety of functional carbonaceous materials from biomass *via* the HTC process have been synthesized with promising prospects in various applications.[3,16]

In this perspective, we discuss the latest advance in the synthesis of functional carbonaceous materials from different biomasses *via* the HTC process. This perspective is mainly composed of two parts. In the first part, the synthesis of carbonaceous materials from crude plant materials and carbohydrates is discussed, either directed or catalyst/template-assisted. In the second part, by citing several detailed discussed cases, we have a rough look at the environmental, catalytic and electrical applications of the carbonaceous and hybrid materials produced under the HTC condition. Finally, we will give the summary and outlook on this active research topic.

2. Hydrothermal synthesis of carbonaceous materials

The HTC process for the synthesis of functional carbonaceous materials from biomass has been intensively studied. Usually, biomass used for this process includes crude plant materials and carbohydrates. Crude plant materials are directly obtained from agricultural residues, wood and herbaceous energy crops, while carbohydrates normally include sugars, starch, hemicellulose, cellulose and other dehydration products of glucose, 2-furaldehyde (furfural) and hydroxymethylfurfural. In the following sections, we will discuss the recent advances in the area of controlled growth and surface functionalization of various carbonaceous materials by the use of crude plant materials or carbohydrates *via* the HTC process (Scheme 1).

2.1 Crude plant materials

2.1.1 Direct hydrothermal carbonization. The direct synthesis of mesoporous carbonaceous nanostructures with bicontinuous porous morphology from crude plant materials[3c] involves an illustrative example as to how the HTC process affects the size, shape and surface structure of carbonaceous materials. The experiment uses the specific products (sugar beet chips, pine cones, pine needles, oak leaves and orange peels) that contain cellulose, hemicelluloses, up to 35% lignins, and smaller amounts of polar polymers as starting materials. After these biomass compounds were heated in sealed autoclaves in the presence of citric acid at 200 °C for 16 h, interestingly two kinds of carbonaceous materials were obtained.

"Soft" plant tissues without an extended crystalline cellulose scaffold yield globular carbonaceous nanoparticles with very small sizes and the porosity is mainly interstitial. For example,

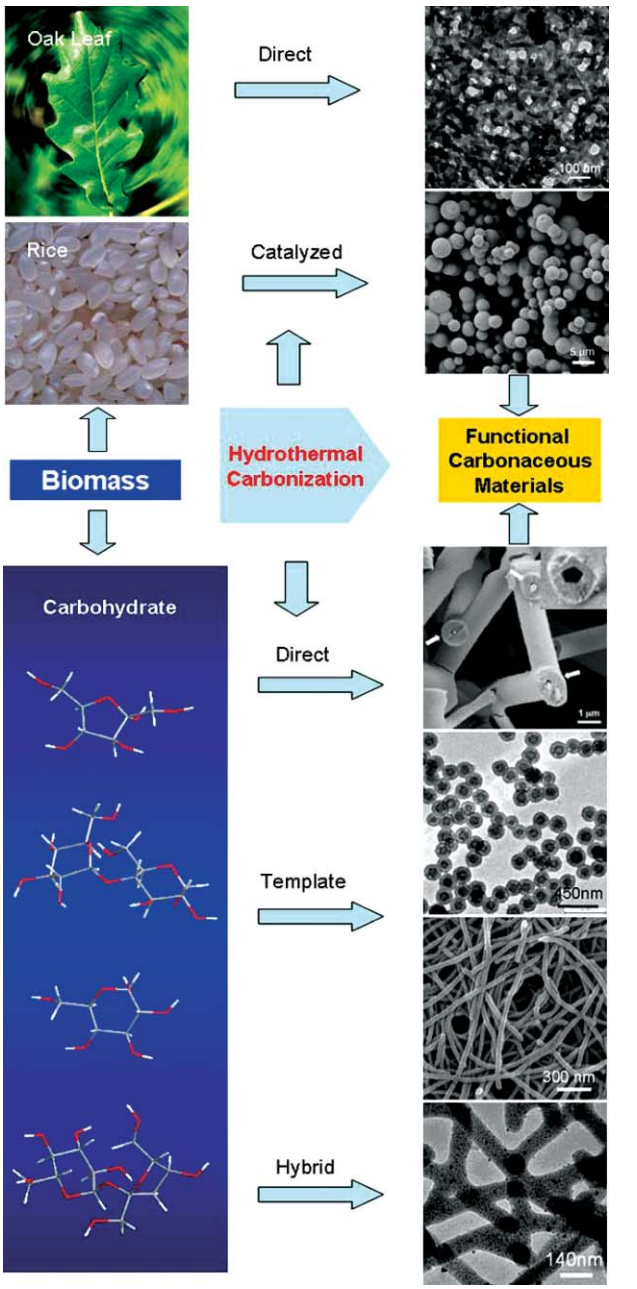

Scheme 1 Schematic illustration of synthesizing various functional carbonaceous materials from biomass and carbohydrates by the hydrothermal carbonization (HTC) process. Functional carbonaceous materials can be synthesized either directly or catalyst/template-assisted from crude plant materials and carbohydrates respectively, by carefully tuning the HTC process and using suitable templates.

being essentially disintegrated and liquefied, the pine needles lose the original structure (Fig. 1a), resulting in a very fine powder comprising 20–200 nm sized globular carbonaceous nanoparticles (Fig. 1b). In addition, it is intriguing to note that the surface of the carbonaceous nanoparticles is highly hydrophilic and easily water-dispersable, owing to the decomposition of other polar components in the biomass.

"Hard" plant tissues with structural, crystalline cellulose scaffolds, however, can preserve outer shape and large-scale structural features on the macro- and microscale; as a result of considerable

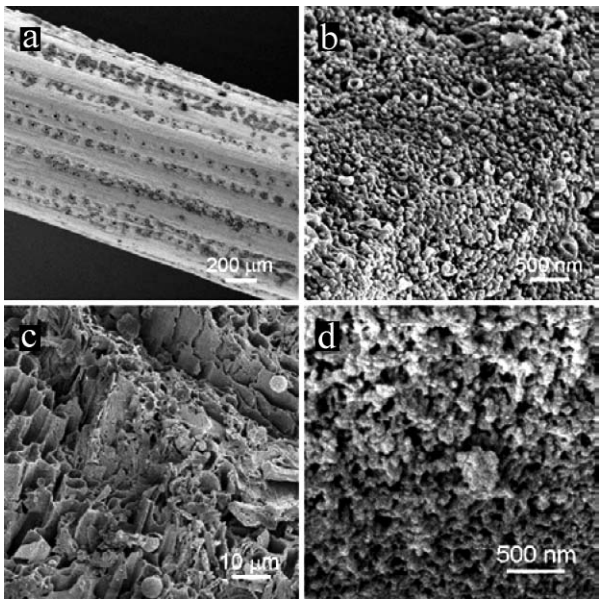

Fig. 1 HRSEM of pine needles (a) before and (b) after being hydrothermally carbonized at 200 °C for 12 h; (c) low-magnification SEM overview of a HTC-treated oak leaf; (d) high-magnification picture of the same HTC- treated oak leaf. Images (a)–(d) reprinted with permission from M. M. Titirici, A. Thomas, S. H. Yu, J. O. Muller and M. Antonietti, *Chem. Mater.*, 2007, **19**, 4205–4212.[3c] © 2007 American Chemical Society.

mass loss, there arises the significant structural change on the nanometer scale, resulting in a sponge-like, bicontinuous carbonaceous network with a well-defined mesoporous structure. As the low-magnified SEM images show, the oak leaves preserve the cellular, layered architecture of the carbohydrate matrix (Fig. 1c). On the other hand, the high-magnified SEM images indicate that the scaffold is rearranged and "opened up" with a well-developed pore system comprising apparent pore sizes from 10 to 100 nm (Fig. 1d). The transmission electron microscopy (TEM) images of a typical, delaminated thin part of the HTC-treated oak leaves (Fig. 2) nicely support the SEM observations of the surface structure of such materials. In addition, the surface of mesoporous carbonaceous materials proved water-wettable, due to the presence of polar groups immobilized at the biocarbon/water interface.

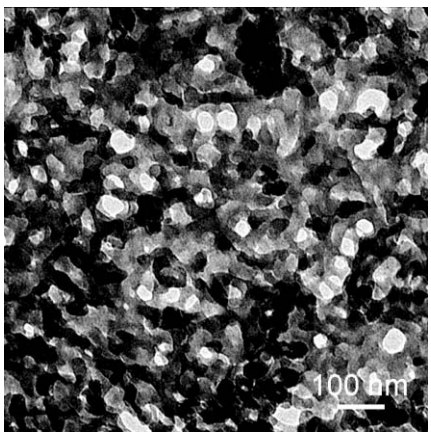

Fig. 2 TEM picture of the local structure HTC-treated oak leaves. Images reprinted with permission from M. M. Titirici, A. Thomas, S. H. Yu, J. O. Muller and M. Antonietti, *Chem. Mater.*, 2007, **19**, 4205–4212.[3c] © 2007 American Chemical Society.

2.1.2 Catalyzed hydrothermal carbonization. It is essential to gain an understanding of the catalysis mechanism in the HTC process during the formation of carbonaceous materials and the associated surface modification. Recently, Yu *et. al.* have reported that hydrothermal carbonization of starch can be effectively accelerated by the presence of metal ions which also directs the synthesis towards various metal–carbon nanoarchitectures, such as Ag@carbon nanocables,[3a] and Ag@carbon-rich composite microcables.[16c] In addition, the presence of $[Fe(NH_4)_2(SO_4)_2]$ can effectively catalyze the carbonization of raw rice grains in the HTC process.[12] The insoluble part of the grain forms larger, porous carbonized species, and preserves the primary grain microstructure, which is different along the body of the grain (Fig. 3a and c). Interestingly, the majority of the 5 nm products are composed of single carbon nanofibers, keeping the primary fibrous structure of the rice tissue on the nanometer scale (Fig. 3b). The soluble fraction forms carbon microspheres (Fig. 3d).

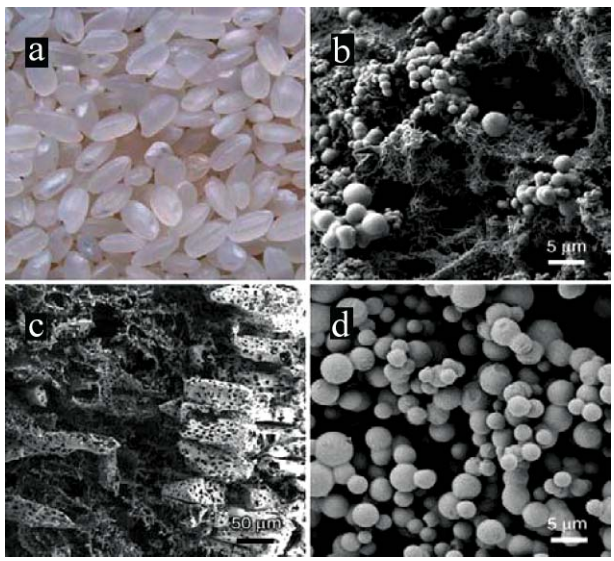

Fig. 3 (a) Photograph of rice grains. (b)–(d) SEM images of the carbonized product: rice grains (5 g), $[Fe(NH_4)_2(SO_4)_2]$ (5 mmol), 200 °C, 12 h, pH 4; (b) coexistence of carbon spheres and a carbonized, microstructured biological tissue; (c) organized carbon scaffold replicating a different biological motif of the nonsoluble carbohydrates in rice; (d) pure carbon spheres collected from the solution generated from the soluble polysaccharides. Images (a)–(d) reprinted with permission from X. J. Cui, M. Antonietti and S. H. Yu, *Small*, 2006, **2**, 756–759.[12] © 2006 Wiley-VCH.

2.2 Carbohydrates

2.2.1 Carbonaceous materials. Traditionally, when sugar or glucose is used as a precursor, the HTC process tends to generate monodispersed colloidal carbon microspheres.[14,15] However, the proper template or additives can control the synthesis of new carbonaceous materials with special and complex structures. A particularly nice case is the synthesis of uniform carbonaceous nanofibers by the HTC process, using glucose and Te nanowires of several nanometers in diameter as starting materials.[16a]

The well-defined ultralong carbon nanofibers can be synthesized by removing the Te nanowires from the Te@carbon-rich composite nanocables with high aspect ratio. The carbonaceous nanofibers have an average diameter of *ca.* 50 nm and up to tens or hundreds of micrometers in length (Fig. 4). The diameter of carbon nanofibers can be easily adjusted by controlling the reaction time of hydrothermal reaction or the ratio of the tellurium and glucose. It must be noted that the high-aspect-ratio structure is the consequence of Te nanowires, which effectively restrain the normal homogeneous nucleation of carbon spheres and promote the heterogeneous deposition of carbonaceous matter on the backbone of Te nanowires to form well-defined Te@carbon-rich composite nanocables. In addition, the Fourier-transform IR (FTIR) spectra also demonstrate that the surface of these carbonaceous nanofibers is highly functionalized, showing high reactivity and reductive behavior.

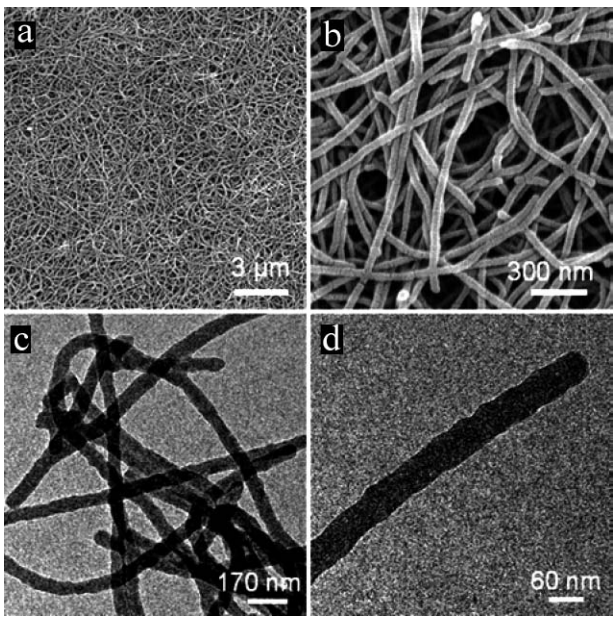

Fig. 4 SEM and TEM images of the carbon nanofibers obtained by removal of the core of the Te@carbon-rich nanocables by treatment with a 30 mL aqueous solution containing 2 mL of hydrochloric acid (36.5 wt%), 5 mL of H_2O_2 (30 wt%), and 20 mL of distilled water ($HCl : H_2O_2 : H_2O$) 2 : 5 : 20, v/v) at room temperature for 12 h. (a) A general view of the nanofibers and (b) an enlarged SEM image. (c)–(d) TEM images of the nanofibers. Images (a)–(d) reprinted with permission from H. S. Qian, S. H. Yu, L. B. Luo, J. Y. Gong, L. F. Fei and X. M. Liu, *Chem. Mater.*, 2006, **18**, 2102–2108.[16a] © 2006 American Chemical Society.

2.2.2 Porous carbonaceous materials. With respect to the use of the HTC process for the fabrication of hierarchical porous carbonaceous materials, it is of the utmost importance that this route not only processes under a simple, low-temperature condition, but synthesizes porous carbonaceous materials with controllable morphology and surface functional groups as well.[17] An attractive instance involves the synthesis of hierarchical carbonaceous materials with functional groups residing at the surface of surface-modified silica templates *via* the HTC process.[3d] In the presence of a silica template, the liquid organic intermediates resulting from dehydration are able to penetrate the pores of the template and to further carbonize in or on the template, forming the complex porous carbonaceous materials.

It is essential to tune the polarity of the template to match that of carbohydrates. As Scheme 2 illustrates, only directed by silica templates with a moderately hydrophobic surface, can hollow spheres composed of a hydrophilic carbon polymer be obtained, whereas dismixing or macroporous carbon casts occur at the presence of templates of hydrophilic surface or very hydrophobic surface, respectively. For moderately hydrophobic silica templates, it is the finite contact angle between the deposited intermediates and the templates that leads to the finally hollow carbon spheres. For mesoporous template, mesoporous carbon shell are obtained by removing the template, with the whole carbonaceous structure composed of *ca* 8–16 nm globular carbon nanoparticles (Fig. 5); for non-porous templates, hollow carbonaceous spheres with a robust carbon coating are observed. Furthermore, the moderately hydrophobic silica template filled with 60 wt% carbon precursor resulted in mesoporous carbonaceous microspheres whereas for that filled with 30 wt% carbon precursor, only small carbon spherules 6–10 nm in size are obtained, owing to the lack of interconnectivity between particles in the coating.

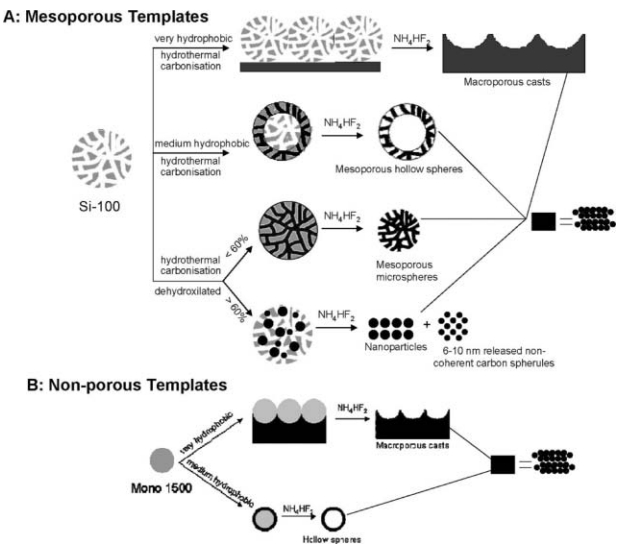

Scheme 2 Schematic representation of the hydrothermal carbonization process in the presence of silica templates with different polarities, leading to various carbon morphologies. Image reprinted with permission from M. M. Titirici, A. Thomas and M. Antonietti, *Adv. Funct. Mater.*, 2007, **17**, 1010–1018.[3d] © 2007 Wiley-VCH.

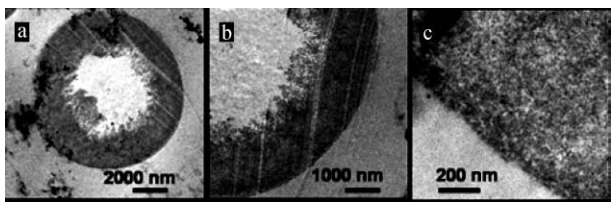

Fig. 5 (a), (b) and (c) Transmission electron microscopy images of the same hollow carbon sphere under different magnifications, resulting from the hydrothermal carbonization of furfural in the presence of mesoporous silica templates with a partly hydrophobized surface. Images (a)–(c) reprinted with permission from M. M. Titirici, A. Thomas and M. Antonietti, *Adv. Funct. Mater.*, 2007, **17**, 1010–1018.[3d] © 2007 Wiley-VCH.

Besides, under the HTC process, the resulting carbonaceous materials remains rich in surface functional groups that are confirmed by FTIR spectroscopy, X-ray photoelectron analysis and water porosimetry, since low temperatures guarantee the surface of a considerable number of functional groups, such as –OH and –C=O groups bonded to the carbon framework. The presence of surface functional groups can greatly improve the hydrophilicity of carbonaceous materials and the stability of their dispersions in aqueous systems.

2.2.3 Hybrid carbonaceous materials. The controlled production of carbonaceous hybrid materials has gradually become a hot and activated topic, motivated by its potential importance to science and technology.[18] We firstly report the controlled synthesis of various metal–carbon nanoarchitectures, such as metal–carbon nanocables, by the HTC process.[3a] Furthermore, we extended this method for the polyvinyl alcohol(PVA)-assisted synthesis of flexible noble metal (Ag, Cu)@carbon-rich composite submicrocables[16c,19] as well as large-scale production of Te@carbon nanocables directed by Te nanowires based on the HTC process.[16a]

It is necessary to illustrate in detail the synthesis of silver–carbon nanocables.[3a] In the HTC process, noble metal salts not only greatly enhance the efficiency and speed of carbonization but are also conducive to the formation of hybrid nanocables with a pentagonal cross-section (Fig. 6a). Such silver–carbon nanocables with lengths as long as 10 μm and diameters of 200–250 nm tend to branch or fuse with each other (Fig. 6a and b). TEM imaging (Fig. 6b) also shows the dimensional ratio measures 2 to 3 between the uniform Ag cores and the carbonaceous sheaths. A probable mechanism of two main steps is also proposed (Scheme 3). In the early stage, tiny silver nanoparticles aggregate, forming chain-like structures with thin walls of an incompletely carbonized gel matrix (Scheme 3a); these precursors aggregate secondarily with simultaneous growth of carbonaceous layers as shells and silver nanowires as cores, producing the final structures (Scheme 3b–d).

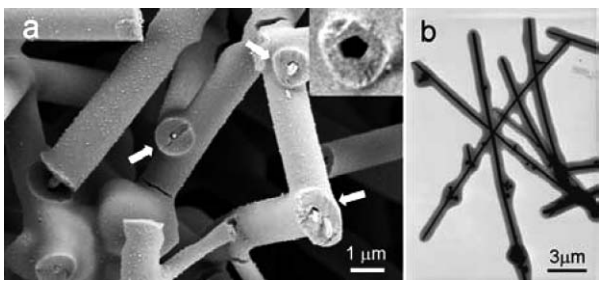

Fig. 6 (a) Typical SEM image of the nanoscale with encapsulated, pentagonal-shaped silver nanowires. The insert shows an incompletely drilled tube with a pentagonal cross-section. (b) TEM image of typical silver–carbon nanocables formed after treating at 160 °C for 12 h: 5 g starch, 5 mmol $AgNO_3$, pH 4. Images (a)–(b) reprinted with permission from S. H. Yu, X. J. Cui, L. L. Li, K. Li, B. Yu, M. Antonietti and H. Colfen, *Adv. Mater.*, 2004, **16**, 1636–1640.[3a] © 2006 Wiley-VCH.

Another particularly nice case is the PVA-assisted synthesis of flexible silver@carbon-rich composite submicrocables.[16c] In this HTC process, silver@carbon-rich composite submicrocables synthesized from different carbon sources, such as glucose, β-cyclodextrin, starch, and maltose, have a core of diameter 150 nm, a shell of thickness 0.8–1.2 μm, and the aspect ratios of most

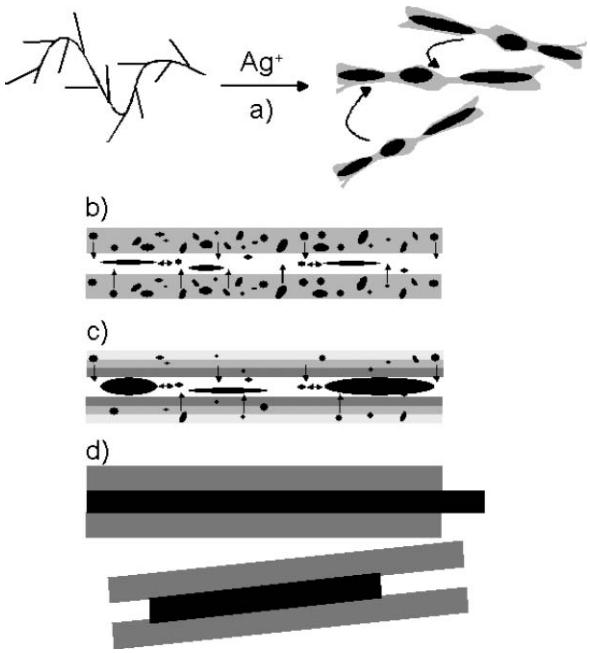

Scheme 3 Schematic formation mechanism of the silver–carbon nanocables. (a) Silver ion reduction by starch leads to silver particles entrapped in a starch-gel matrix. (b) Secondary aggregation of several gel-strings shown in (a) and the start of the silver-catalyzed carbonization reactions. The graphite formation perpendicular to the silver interfact leads to a partially hollow structure due to the limited pliability of organized graphite platelets. Simultaneously, silver particles move into the hollow interior and fuse with the existing ones *via* an oriented attachment mechanism. The arrows are representative of the movement for each particle. (c) Continuation of this process leads to elongated silver structures in the hollow carbon cable interior which is forming, until (d) the silver rods fuse in a crystallographically oriented way to produce the nanocables, while the wall finishes carbonization. Image reprinted with permission from S. H. Yu, X. J. Cui, L. L. Li, K. Li, B. Yu, M. Antonietti and H. Colfen, *Adv. Mater.*, 2004, **16**, 1636–1640.[3a] © 2006 Wiley-VCH.

composite cables range from 30 to 50 (Fig. 7). Importantly, the FTIR spectra shows that the surface of the composite submicrocables contains rich functional groups, such as –OH and –C=O groups. Furthermore, in the whole HTC process, PVA molecules play vital roles, acting as a capping reagent, guiding the oriented growth of microcables as well as effectively catalyzing polymerization and carbonization of these carbohydrates. In addition, this process is extended to the synthesis of other

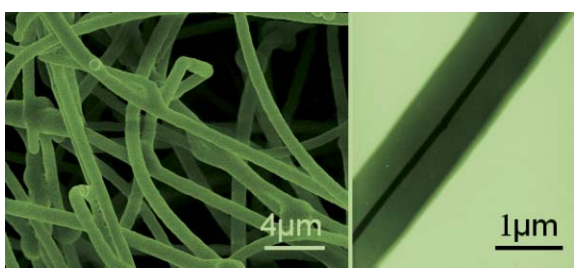

Fig. 7 TEM overview images of silver@carbon-rich composite submicrocables from 0.5 g glucose, at 180 °C for 4 days. Images reprinted with permission from L. B. Luo, S. H. Yu, H. S. Qian and J. Y. Gong, *Chem. Commun.*, 2006, 793–795.[16c] © 2006 Royal Society of Chemistry.

carbonaceous materials, such as copper@carbon-rich composite submicrocables and carbonaceous submicrotubes.[20]

Meanwhile, the synthesis of SiO_2@C microspheres is also very attractive.[21] In this HTC process, uniform and functionalized SiO_2@C microspheres can be synthesized with glucose as carbon precursor and silica spheres as cores. A surprising feature of the product is that there exists a vacant region between the carbon shells and silica cores (Fig. 8). Such SiO_2@C core-shell spheres can be further applied to prepare SiO_2@C@SiO_2, SiO_2@SiO_2 with vacant region between two SiO_2 shells, noble metal nanoparticles loaded on SiO_2@C core–shell spheres, and hollow carbon capsules through different synthetic processes. Furthermore, the surfaces of SiO_2@C microspheres are highly functionalized, display excellent chemical reactivity, and are able to reduce *in situ* noble-metal ions to nanoparticles and load them onto the surface. These unique core–shell hybrid spherical composites could find applications as catalyst supports, adsorbents, encapsulation, biomolecule reactors and reaction templates.

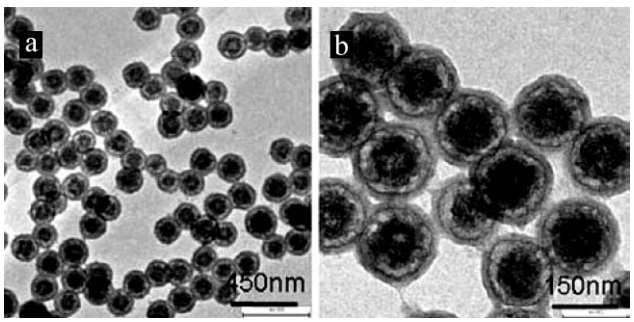

Fig. 8 TEM images of representative SiO_2@C core–shell micropheres. Images (a) and (b) reprinted with permission from Y. Wan, Y. L. Min and S. H. Yu, *Langmuir*, 2008, **24**, 5024–5028.[21] © 2008 American Chemical Society.

From the discussion above, we can see that the HTC process is a promising method of the synthesis of various interesting carbonaceous materials from biomass. Yet it must be noted that other methods also perform well or even better in certain occasions, *e.g.* based on the combination of a solvothermal route and a mild self-assembly approach, carbon-rich submicrotubes can be synthesized (Fig. 9).[10,22] Amorphous carbonaceous nanoparticles with functional groups are firstly produced by the carbonization of glucose in pyridine solution, then these nanoparticles can self-assemble into submicrotubes by mixing the resulting solution with water.

3. Applications of the carbonaceous materials

The existing and promising applications of carbonaceous and hybrid materials made from the HTC process include carbon fixation, chromatography, catalyst supports, gas-selective adsorbents, drug delivery and electrode materials.[23] The HTC process of biomass is currently the most efficient process, with "carbon efficiency" close to 1, to remove atmospheric CO_2, which can be bound into carbonaceous materials. Based on the HTC process, rich functional groups remaining on the surface of various carbonaceous or hybrid materials can facilitate loading of noble metal nanoparticles used as catalysts. Besides, the superior storage

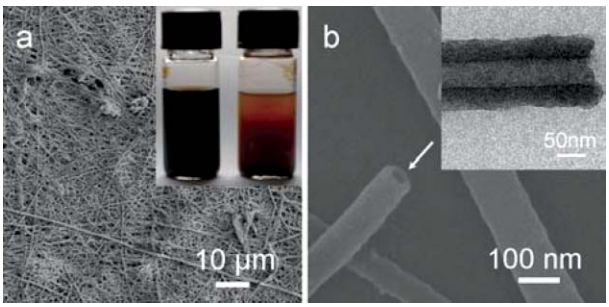

Fig. 9 SEM and TEM images of the carbon-rich composite submicrotubes. (a) A general overview of the submicrotubes. The insert photograph image is untreated solution (left) and after self-assembly the prepared sample redispersed in distilled water (right). (b) High-magnification SEM images, clearly showing the open ends of these tubes. The insert TEM image shows the tube structure. Images (a) and (b) reprinted with permission from Y. J. Zhan and S. H. Yu, *J. Phys. Chem. C*, 2008, **112**, 4024–4028.[10] © 2008 American Chemical Society.

performance of the carbonaceous hybrid materials made from the HTC process makes them suitable as anode material for lithium-ion batteries.

3.1 Environmental applications

Given climate changes and the role of CO_2 therein, it would be necessary not only to slow down further CO_2 emissions but also to develop a chemical "CO_2 disposal" industry for sequestering the atmospheric CO_2 from industrialization of past years. The coalification of biomass, the biggest carbon converter with the highest efficiency to bind CO_2 away from the atmosphere, by the HTC process, has a potential to function as the most efficient tool for this target.[3b] First, the desirable acceleration of the coalification of biomass by a factor of 10^6–10^9 makes it a technically attractive, realistic "artificial" instrument for fixing the carbon of biomass on large scales. Second, it is the most efficient strategy for carbon fixation, with a "carbon efficiency" close to 1 (Fig. 10).[3b] Also, compared to the traditional high-temperature carbonization

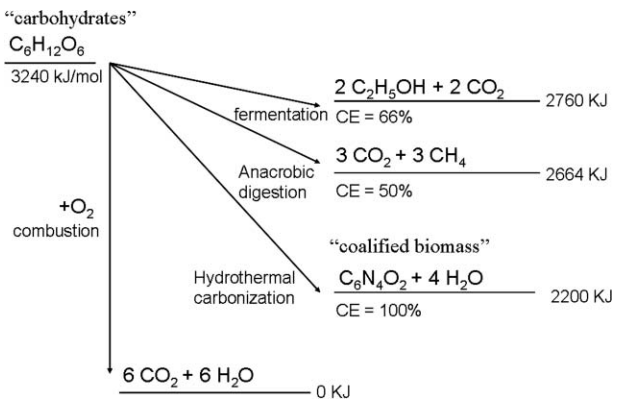

Fig. 10 Comparison of different energy and carbon exploitation schemes from carbohydrates, based on the stored combustion energy and the "carbon efficiency" of the transformation (CE). The "sum formula" of the coalified plant material is a schematic simplification. The image is reprinted with permission from M. M. Titirici, A. Thomas and M. Antonietti, *New J. Chem.*, 2007, **31**, 787–789.[3b] © 2007 Royal Society of Chemistry.

reactions, the HTC route processes under a mild condition with low-temperature ($\leq$ 200 °C), and the high exothermic characteristic (*i.e.* liberating about a third of the combustion energy of the sugars) further promotes the reaction with ease (Fig. 10). Therefore, the HTC process qualifies as an attractive technique to handle a significant part of the CO_2 problem.

3.2 Catalytic applications

Nanostructured carbonaceous materials, such as carbon nanotubes,[24] nanofibers,[25] nanocoils,[26] active carbon,[27] and other carbon nanomaterials[28] loaded with noble metal nanocatalysts, have attracted much interest for their extensive applications proposed in catalysis.[29] Recently, using the HTC process, our group have successfully synthesized the so-called "hybrid fleece" structures,[16b] *i.e.* uniform carbonaceous nanofibers embedded with noble-metal nanoparticles that show different average diameter and distribution for different metals (Fig. 11). These nanoparticles are loaded in the nanofibers *via* the reduction of the noble-metal salts by the functional groups rich in the surface of carbonaceous nanofibers, such as –OH and –C=O groups. Importantly, the resulting hybrid nanostructures perform as efficient catalysts for the 100% conversion of CO to CO_2 at low temperature, due to their thermal, chemical, and mechanical stability, nano- and microstructure speciality, the presence of binary carbon–metal contacts, and their high specific metal surface area. It must be noted that the second run of catalysis tests has been better performed than was the first run. This phenomenon indicates that the truly active species are formed during the first heating and oxidation cycle. As Fig. 9a shows, the C–Pd system can completely convert CO to CO_2 at 210 °C in the second run, lower than the temperature of the first run (250 °C). Also, the catalytic activity depends sensitively on the type of metal loading, among which the Pt system has the most efficiency (Fig. 12).

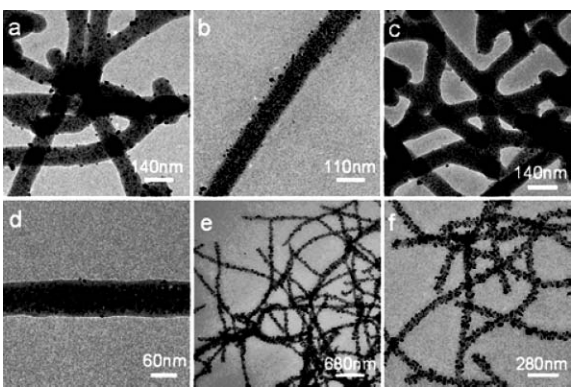

Fig. 11 TEM images showing noble-metal nanoparticles loaded on the surfaces of carbon nanofibers. (a), (b) Pd nanoparticles with an average diameter of *ca.* 6 nm; (c), (d) Pt nanoparticles with an average diameter of *ca.* 7 nm; the nanoparticles are well dispersed within the fiber bodies and on the outside surface; and (e), (f) Au nanoparticles ranging from 7 to 15 nm in diameter; most of the Au nanoparticles adsorbed on the outside surfaces of the carbon nanofibers. Images (a)–(f) reprinted with permission from H. S. Qian, M. Antonietti and S. H. Yu, *Adv. Funct. Mater.*, 2007, **17**, 637–643.[16b] © 2007 Wiley-VCH.

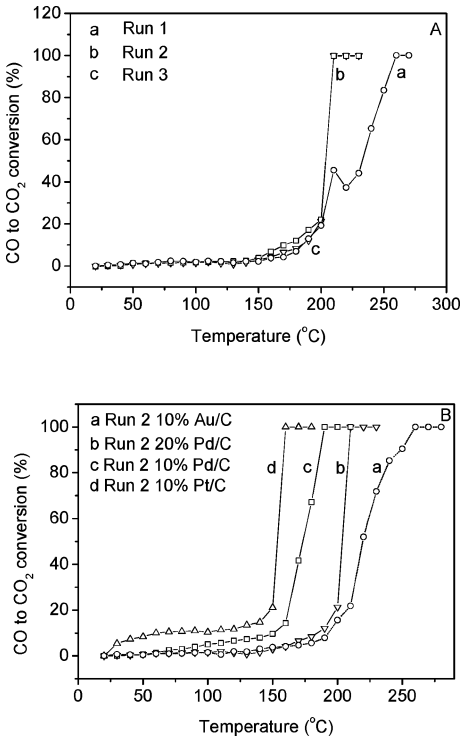

Fig. 12 (A) CO conversion efficiencies of three runs with as-obtained C–Pd as the catalyst. (B) CO conversion efficiencies of the second run with different as-obtained noble-metal catalysts supported by carbon nanofibers: (a) 10 wt% C–Au; (b) 20 wt% C–Pd; (c) 10 wt% C–Pd; (d) 10 wt% C–Pt. Images (a) and (b) reprinted with permission from H. S. Qian, M. Antonietti and S. H. Yu, *Adv. Funct. Mater.*, 2007, **17**, 637–643.[16b] © 2007 Wiley-VCH.

Another exciting example is the synthesis of a novel metal–carbon nanocomposite catalyst, which can convert phenol into cyclohexanone highly selectively, through the HTC process.[29] In this approach, the noble metal salt is reduced by the carbon source of furfural, yielding Pd@hydrophilic-C spheres (Fig. 13a). Compared with the commercial hydrophobic charcoal-supported catalyst, this catalyst shows good selectivity towards partial hydrogenation, generating mainly cyclohexanone rather than cyclohexanol (Fig. 13b). A possible mechanism is that the hydrophobic cyclohexanone is displaced from the hydrophilic pores of the carbonaceous shells and thus is prevented from further hydrogenation into cyclohexane.

3.3 Electrical applications

Recent reports have demonstrated that the anode of silicon–carbon composites can combine the advantageous properties of carbon (long cycle life) with silicon (high lithium-storage capacity), leading to great improvement of the overall electrochemical performance of the anode of lithium-ion batteries.[30] The Si@SiO_x–C nanocomposite has been synthesized *via* a facile and green HTC process, showing superior lithium-storage capacity.[16d] The synthesized nanocomposite presents a core–shell structure (*ca.* 50 nm in size) with a silica core wrapped by a coating layer of SiO_x and C around 10 nm in thickness (Fig. 14), and it owns properties of both sufficient conductivity and mechanical stability. Compared with

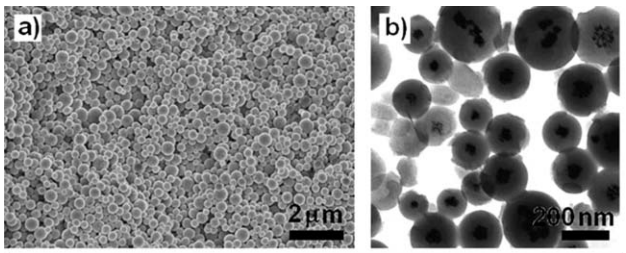

c)

Catalyst	Time/h	Conversion (%)	Selectivity (%) Cyclohexanol	Cyclohexanone
Pd@hydrophilic-C	10	60	—	>99
Pd@hydrophilic-C	20	>99	5	95
Pd@hydrophilic-C	72	>99	50	50
Pd@hydrophilic-C[b]	20	45	30	70
10% Pd@C	20	100	100	0
10% Pd@C	1	100	100	0
10% Pd@Al_2O_3	20	100	100	0

[a] In a typical reaction, 50 mg of catalyst were added to 100 mg of phenol and the Mixture was heated to 100 °C under 1 Mpa of hydrogen pressure. [b] Reference test in cyclohexane.

Fig. 13 (a) and (b) SEM image and TEM images of Pd@hydrophilic-C. (c) Catalytic activity of differently supported Pd for the hydrogenation of phenol.[a] Images (a)–(c) reprinted with permission from P. Makowski, R. D. Cakan, M. Antonietti, F. Goettmann and M. M. Titirici, *Chem. Commun.*, 2008, 999–1001.[29] © 2008 Royal Society of Chemistry.

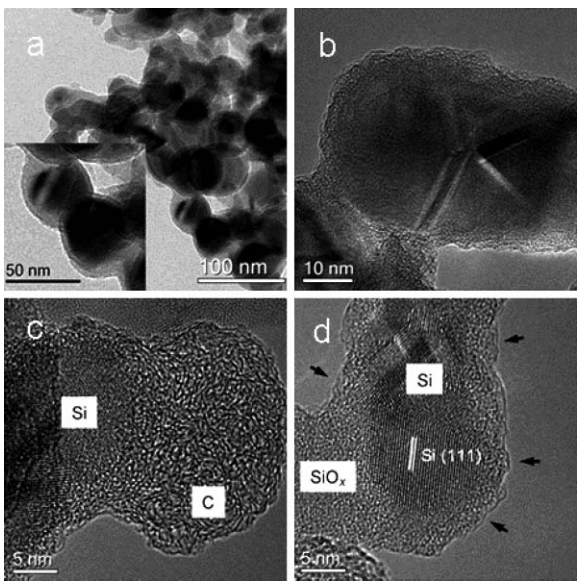

Fig. 14 TEM images of the Si@SiO_x–C nanocomposite produced by hydrothermal carbonization and further carbonization at 750 °C under N_2. (a) Overview of the Si@SiO_x–C nanocomposites and a TEM image at higher magnification (in the inset) showing uniform sphere-like particles; (b) HRTEM image clearly showing the core–shell structure; (c), (d) HRTEM image displaying details of the silicon nanoparticles coated with SiO_x and carbon. Images (a)–(d) reprinted with permission from Y. S. Hu, D. C. Rezan, M. M. Titirici, J. O. Muller, R. Schlogl, M. Antonietti and J. Maier, *Angew. Chem., Int. Ed.*, 2008, **47**, 1645–1649.[16d] © 2008 Wiley-VCH.

other electrode–electrolyte systems, Si@SiO_x–C nanocomposite in vinylene carbonate (VC) shows remarkably improved lithium-storage performance in terms of highly reversible lithium-storage performance (1100 mAh g^{-1}), excellent cycling performance, and high rate capability (Fig. 15). The good cycling performance may be mainly due to the formation of a solid electrolyte interphase (SEI) on the particle surface, caused by the reduction of the electrolyte. And the SEI hinders further loss of irreversible capacity after the first charge–discharge cycle.[16d]

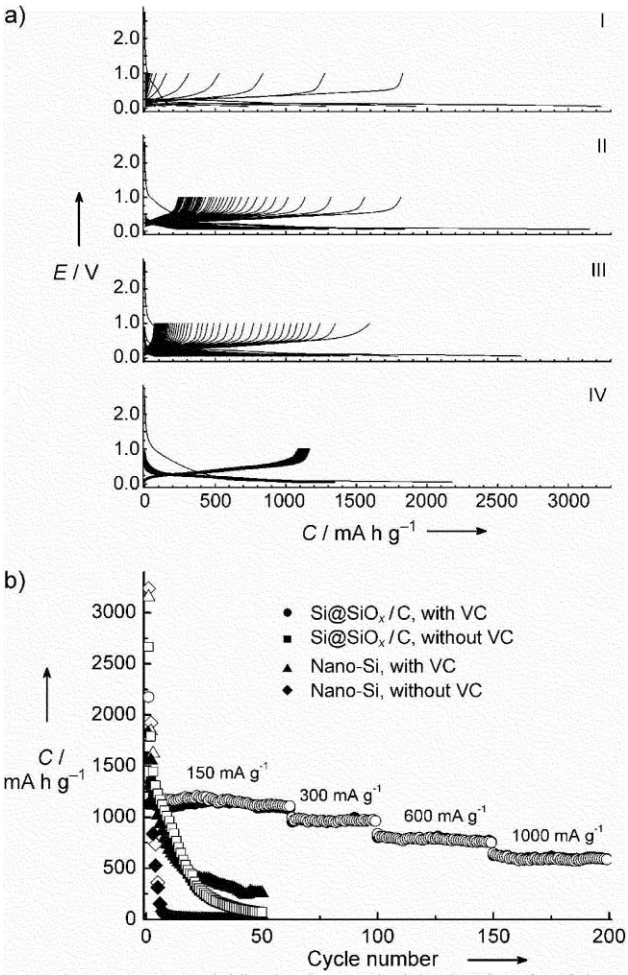

Fig. 15 (a) Galvanostatic discharge–charge curves (Li insertion, voltage decreases; Li extraction, voltage increases, respectively) of pure Si nanoparticles (I, II) and Si@SiO_x–C nanocomposite (III, IV) electrodes cycled at a current density of 150 mA g^{-1} between voltage limits of 0.05–1 V in VC-free (I, III) and VC-containing (II, IV) 1 M $LiPF_6$ in EC–DMC solutions. (b) Cycling and rate performance of pure Si nanoparticles and Si@SiO_x–C nanocomposite electrodes cycled in VC-free and VC-containing 1 M $LiPF_6$ in EC–DMC solutions (solid symbols: charge; empty symbols: discharge.). Images (a) and (b) reprinted with permission from Y. S. Hu, D. C. Rezan, M. M. Titirici, J. O. Muller, R. Schlogl, M. Antonietti and J. Maier, *Angew. Chem., Int. Ed.*, 2008, **47**, 1645–1649.[16d] © 2008 Wiley-VCH.

4. Summary and outlook

The synthesis of various carbonaceous structures discussed in this perspective all originate from biomass *via* the HTC process. Although differences among them (that some cases require metal

ions as catalyst while some others rely on template to form specific shapes) couldn't be ignored, there do exist significant common features: high efficiency for the synthesis of carbonaceous materials, active surface rich in functional groups, and "green" sources from biomass, *etc.*

Importantly, the resulting structures are not only of aesthetic and/or theoretical value, but of practical application potential as well. The synthesized carbonaceous materials find their place in a variety of application areas: solving the environmental problem of CO_2, catalyzing conversion from CO to CO_2, improving the organic reaction efficiency and selectivity, and improving the electrochemical performance of an anode, owing to their distinctive characteristic from the HTC process of biomass.

Although the HTC process has been a prominent success in the synthesis of many carbonaceous materials of distinctive structures and rich functional groups, there still remains a blank as to the components of the final products and the mechanism of detailed process. Yet human beings have never been satisfied on the arduous journey for the pursuing of truth of "why this is the case". Further exploration in these areas will facilitate the rational design of a variety of functional carbonaceous materials with an ideal hierarchy when we gradually uncover the mysterious veil of the mechanism behind hydrothermal carbonization reaction.

Acknowledgements

S.-H. Yu acknowledges the funding support from the National Science Foundation of China (NSFC) (Grant Nos. 50732006, 20325104, 20621061, 20671085), the Partner-Group of the Chinese Academy of Sciences—the Max Planck Society, the 973 project (2005CB623601), Anhui Development Fund for Talent Personnel and Anhui Education Committee (2006Z027, ZD2007004-1), the Scientific Research Foundation for the Returned Overseas Chinese Scholars, and the Specialized Research Fund for the Doctoral Program (SRFDP) of Higher Education State Education Ministry.

References

1 H. W. Kroto, J. R. Heath, S. C. Brien, R. F. Curl and R. E. Smalley, *Nature*, 1985, **318**, 162–163.
2 S. Iijima, *Nature*, 1991, **354**, 56–58.
3 (*a*) S. H. Yu, X. J. Cui, L. L. Li, K. Li, B. Yu, M. Antonietti and H. Colfen, *Adv. Mater.*, 2004, **16**, 1636–1640; (*b*) M. M. Titirici, A. Thomas and M. Antonietti, *New J. Chem.*, 2007, **31**, 787–789; (*c*) M. M. Titirici, A. Thomas, S. H. Yu, J. O. Muller and M. Antonietti, *Chem. Mater.*, 2007, **19**, 4205–4212; (*d*) M. M. Titirici, A. Thomas and M. Antonietti, *Adv. Funct. Mater.*, 2007, **17**, 1010–1018.
4 (*a*) K. Sanderson, *Nature*, 2006, **444**, 673–676; (*b*) T. H. Deluca, *Science*, 2006, **312**, 1743–1744; (*c*) M. Downing, *Science*, 2006, **312**, 1745–1746; (*d*) D. Connor and I. Minguez, *Science*, 2006, **312**, 1743–1743; (*e*) T. Dalgaard, U. Jorgensen, J. E. Olesen, E. S. Jensen and E. S. Kristensen, *Science*, 2006, **312**, 1743–1743; (*f*) S. E. Koonin, *Science*, 2006, **312**, 1744–1744; (*g*) M. W. Palmer, *Science*, 2006, **312**, 1745–1745.
5 (*a*) K. R. Brower, *Science*, 2006, **312**, 1744–1744; (*b*) C. J. Cleveland, C. A. S. Hall and R. A. Herendeen, *Science*, 2006, **312**, 1746–1746; (*c*) B. H. Davison, A. J. Ragauskas, R. Templer, T. J. Tschaplinski and J. R. Mielenz, *Science*, 2006, **312**, 1744–1745; (*d*) E. Farrell, R. J. Plevin, B. T. Turner, A. D. Jones, M. O'Hare and D. M. Kammen, *Science*, 2006, **312**, 1747–1748; (*e*) A. E. Farrell, R. J. Plevin, B. T. Turner, A. D. Jones, M. O'Hare and D. M. Kammen, *Science*, 2006, **311**, 506–508; (*f*) A. E. Farrell, *Science*, 2006, **312**, 1748–1748; (*g*) R. K. Kaufmann, *Science*, 2006, **312**, 1747–1747.
6 (*a*) J. Lehmann, *Nature*, 2007, **447**, 143–144; (*b*) D. R. Dodds and R. A. Gross, *Science*, 2007, **318**, 1250–1251; (*c*) A. J. Ragauskas, C. K. Williams, B. H. Davison, G. Britovsek, J. Cairney, C. A. Eckert, W. J. Frederick, J. P. Hallett, D. J. Leak, C. L. Liotta, J. R. Mielenz, R. Murphy, R. Templer and T. Tschaplinski, *Science*, 2006, **311**, 484–489.
7 (*a*) L. D. Schmidt and P. J. Dauenhauer, *Nature*, 2007, **447**, 914–915; (*b*) L. Lynd, N. Greene, B. Dale, M. Laser, D. Lashof, M. Wang and C. Wyman, *Science*, 2006, **312**, 1746–1747; (*c*) T. W. Patzek, *Science*, 2006, **312**, 1747–1747; (*d*) D. Tilman, J. Hill and C. Lehman, *Science*, 2006, **314**, 1598–1600; (*e*) N. Hagens, R. Costanza and K. Mulder, *Science*, 2006, **312**, 1746–1746.
8 (*a*) A. Thess, R. Lee, P. Nikolaev, H. J. Dai, P. Petit, J. Robert, C. H. Xu, Y. H. Lee, S. G. Kim, A. G. Rinzler, D. T. Colbert, G. E. Scuseria, D. Tomanek, J. E. Fischer and R. E. Smalley, *Science*, 1996, **273**, 483–487; (*b*) M. Joseyacaman, M. Mikiyoshida, L. Rendon and J. G. Santiesteban, *Appl. Phys. Lett.*, 1993, **62**, 657–659; (*c*) M. Joseyacaman, H. Terrones, L. Rendon and J. M. Dominguez, *Carbon*, 1995, **33**, 669–678; (*d*) L. Gherghel, C. Kubel, G. Lieser, H. J. Rader and K. Mullen, *J. Am. Chem. Soc.*, 2002, **124**, 13130–13138; (*e*) Y. D. Li, Y. T. Qian, H. W. Liao, Y. Ding, L. Yang, C. Y. Xu, F. Q. Li and G. Zhou, *Science*, 1998, **281**, 246–247.
9 (*a*) Y. Gogotsi, J. A. Libera and M. Yoshimura, *J. Mater. Res.*, 2000, **15**, 2591–2594; (*b*) J. Libera and Y. Gogotsi, *Carbon*, 2001, **39**, 1307–1318; (*c*) Y. Gogotsi, J. A. Libera, A. Guvenc-Yazicioglu and C. M. Megaridis, *Appl. Phys. Lett.*, 2001, **79**, 1021–1023; (*d*) Y. Gogotsi, N. Naguib and J. A. Libera, *Chem. Phys. Lett.*, 2002, **365**, 354–360; (*e*) Y. G. Gogotsi and M. Yoshimura, *Nature*, 1994, **367**, 628–630.
10 Y. J. Zhan and S. H. Yu, *J. Phys. Chem. C*, 2008, **112**, 4024–4028.
11 G. Demazeau, *J. Mater. Chem.*, 1999, **9**, 15–18.
12 X. J. Cui, M. Antonietti and S. H. Yu, *Small*, 2006, **2**, 756–759.
13 (*a*) F. Bergius, *Die Anwendung hoher Drucke Bei chemischen Vorgangen und eine Nachbidung des Entstehungsprozesses der Steinkohle*, Verlag Wilhelm Knapp, Halle an der Saale, Germany, 1913; (*b*) E. Berl and A. Schmidt, *Justus Liebigs Ann. Chem.*, 1932, **493**, 97–123; (*c*) E. Berl, A. Schmidt and H. Koch, *Angew. Chem.*, 1932, **45**, 0517–0519; (*d*) J. P. Schuhmacher, F. J. Huntjens and D. W. Vankrevelen, *Fuel*, 1960, **39**, 223–234.
14 Q. Wang, H. Li, L. Q. Chen and X. J. Huang, *Carbon*, 2001, **39**, 2211–2214.
15 X. M. Sun and Y. D. Li, *Angew. Chem., Int. Ed.*, 2004, **43**, 597–601.
16 (*a*) H. S. Qian, S. H. Yu, L. B. Luo, J. Y. Gong, L. F. Fei and X. M. Liu, *Chem. Mater.*, 2006, **18**, 2102–2108; (*b*) H. S. Qian, M. Antonietti and S. H. Yu, *Adv. Funct. Mater.*, 2007, **17**, 637–643; (*c*) L. B. Luo, S. H. Yu, H. S. Qian and J. Y. Gong, *Chem. Commun.*, 2006, 793–795; (*d*) Y. S. Hu, D. C. Rezan, M. M. Titirici, J. O. Muller, R. Schlogl, M. Antonietti and J. Maier, *Angew. Chem., Int. Ed.*, 2008, **47**, 1645–1649.
17 (*a*) T. W. Kim and L. A. Solovyov, *J. Mater. Chem.*, 2006, **16**, 1445–1455; (*b*) Y. C. Liang, M. Hanzlik and R. Anwander, *J. Mater. Chem.*, 2006, **16**, 1238–1253; (*c*) M. M. Titirici, A. Thomas and M. Antonietti, *J. Mater. Chem.*, 2007, **17**, 3412–3418; (*d*) J. Wang, J. C. Groen, W. Yue, W. Zhou and M. O. Coppens, *J. Mater. Chem.*, 2008, **18**, 468–474.
18 (*a*) J. C. Yu, X. L. Hu, Q. Li and L. Z. Zhang, *Chem. Commun.*, 2005, 2704–2706; (*b*) B. Deng, A. W. Xu, G. Y. Chen, R. Q. Song and L. P. Chen, *J. Phys. Chem. B*, 2006, **110**, 11711–11716; (*c*) X. M. Sun and Y. D. Li, *Langmuir*, 2005, **21**, 6019–6024.
19 J. Y. Gong, L. B. Luo, S. H. Yu, H. S. Qian and L. F. Fei, *J. Mater. Chem.*, 2006, **16**, 101–105.
20 J. Y. Gong, S. H. Yu, H. S. Qian, L. B. Luo and T. W. Li, *J. Phys. Chem. C.*, 2006, **16**, 101–105.
21 Y. Wan, Y. L. Min and S. H. Yu, *Langmuir*, 2008, **24**, 5024–5028.
22 S. S. Feng, M. L. Zhu, L. P. Lu and M. L. Guo, *Chem. Commun.*, 2007, 4785–4787.
23 H. Orikasa, J. Karoji, K. Matsui and T. Kyotani, *Dalton Trans.*, 2007, 3757–3762.
24 W. Z. Li, C. H. Liang, J. S. Qiu, W. J. Zhou, H. M. Han, Z. B. Wei, G. Q. Sun and Q. Xin, *Carbon*, 2002, **40**, 791–794.
25 D. A. Bulushev, I. Yuranov, E. I. Suvorova, P. A. Buffat and L. Kiwi-Minsker, *J. Catal.*, 2004, **224**, 8–17.

26 T. Hyeon, S. Han, Y. E. Sung, K. W. Park and Y. W. Kim, *Angew. Chem., Int. Ed.*, 2003, **42**, 4352–4356.
27 J. Prabhuram, X. Wang, C. L. Hui and I. M. Hsing, *J. Phys. Chem. B*, 2003, **107**, 11057–11064.
28 S. H. Joo, S. J. Choi, I. Oh, J. Kwak, Z. Liu, O. Terasaki and R. Ryoo, *Nature*, 2001, **412**, 169–172.
29 P. Makowski, R. D. Cakan, M. Antonietti, F. Goettmann and M. M. Titirici, *Chem. Commun.*, 2008, 999–1001.
30 (*a*) X. D. Wu, Z. X. Wang, L. Q. Chen and X. J. Huang, *Electrochem. Commun.*, 2003, **5**, 935–939; (*b*) J. Yang, B. F. Wang, K. Wang, Y. Liu, J. Y. Xie and Z. S. Wen, *Electrochem. Solid-State Lett.*, 2003, **6**, A154–A156; (*c*) S. H. Ng, J. Z. Wang, D. Wexler, K. Konstantinov, Z. P. Guo and H. K. Liu, *Angew. Chem., Int. Ed.*, 2006, **45**, 6896–6899; (*d*) M. Holzapfel, H. Buqa, W. Scheifele, P. Novak and F. M. Petrat, *Chem. Commun.*, 2005, 1566–1568.